# Assessing Rotation/Curvature-Corrected Eddy-Viscosity Models for the Computation of Centrifugal-Compressor Flows

G. Dufour,* J.-B. Cazalbou, X. Carbonneau, and P. Chassaing[†]

*ENSICA, 1 pl. Émile Blouin, 31056 Toulouse Cedex 5, France*

(Dated: December 10, 2007)

## Abstract

Rotation and curvature (RC) effects on turbulence are expected to impact losses and flow structure in turbomachines. This paper examines two recent eddy-viscosity-model corrections devised to account for these effects: the Spalart and Shur [Aerospace Sc. Tech., 1:5 (1997)] correction to the model of Spalart & Allmaras, and the correction of Cazalbou *et al.* [Phys. Fluids, 17:055110 (2005)] to the $(k, \epsilon)$ model. The method of verification and validation is applied to assess the impact of these corrections on the computation of a centrifugal-compressor test case. First, a review of RC effects on turbulence as they apply to centrifugal compressors is made. The two corrected models are then presented. Second, the *Radiver* open test case [Ziegler *et al.*, ASME Trans. J. Turbo. 125:173-183 (2003)] is used as a basis for the assessment of the two corrections. After a physical-consistency analysis, the Richardson extrapolation is applied to quantify the numerical errors involved in all the calculations. Finally, experimental data are used to perform validation for both global and local predictions. The consistency analysis shows that both corrections lead to significant changes in the turbulent field, in perfect agreement with the underlying theoretical considerations. The uncertainty analysis shows that the predictions of the global performances are more sensitive to grid refinement than they are to RC turbulence modeling. However, the opposite conclusion is drawn with regard to the prediction of some local flow properties: improvements are obtained with the RC corrections, the best results being observed for the RC-corrected $(k, \epsilon)$ model.

---

*Electronic address: `gdufour@ensica.fr`; Now at: CERFACS, CFD Team, Toulouse, France.

[†]Also at INPT-ENSEEIHT-Institut de Mécanique des Fluides de Toulouse UMR 5502 CNRS, France.

# I. INTRODUCTION

Flows in turbomachines, and particularly in centrifugal compressors, are recognized as being very complex, due to important viscous and three-dimensional effects, with a significant contribution of the turbulence properties. As mentioned in reviews by Lakshminarayna [1] and Bradshaw [2], the main challenges with regard to the underlying turbulence physics are the prediction of the effects of compressibility, pressure gradients or transition, and the effects of system rotation and streamline curvature (further referred to as RC effects). In this study, we shall focus on the modeling of the effects of rotation and curvature in centrifugal compressors.

Our basic knowledge of RC effects on turbulence is quite fair for simple configurations, where they are responsible for strong modifications to the fluctuating field: they can induce either an enhancement ("destabilization") or a reduction ("stabilization") of the turbulent activity [3, 4]. In centrifugal impellers, streamline curvature is caused by the geometry and by secondary flows (including tip leakage). Rotation is particularly important in small-size or high-pressure-ratio rotors, which need to be operated at high rotation speed. It is therefore expected that RC effects on turbulence significantly impact losses and flow structure in centrifugal impellers. In particular, Baljé [5] conjectured a significant contribution of rotation effects to the formation of the jet/wake structure at the outlet of a centrifugal rotor. Computational Fluid Dynamics (CFD) can be used to improve our understanding of these issues. Moore and Moore [6] tackled this problem for the NASA Low Speed Centrifugal Compressor: they observed significant changes of the turbulent field, but a rather limited impact on the mean-flow characteristics. However, their computations were made with a simple modification of a mixing-length model. Generally speaking, most of the early corrections for RC effects were valid only for mild curvature and rotation. This motivates further investigations with current advanced turbulence modeling strategies.

In the present study, we shall examine two recent model corrections devised specifically to account for RC effects: the correction proposed by Spalart and Shur [7] applied to the Spalart & Allmaras model (SA) [8]; and the two-equation-model correction of Cazalbou *et al* [9], applied here to the $(k, \epsilon)$ model of Yang & Shih (YS) [10]. The RC-corrected versions of these two models will further be referred to as SARC and YSRC, respectively.

The primary objectives of the present study are: to assess the capability of the SARC

and YSRC models to reproduce RC effects on turbulence in a centrifugal compressor; and to quantify the global impact of RC modeling, through a comprehensive comparison against detailed experimental data. Actually quantitative assessment of the benefit of the corrections can be guaranteed by the use of uncertainty analysis within the verification and validation (V&V) framework. The rest of the paper is organized as follows: (i) section II provides a theoretical analysis of RC effects on turbulence in a radial impeller, together with a brief presentation of the corrections, which are then used to make a consistency analysis of the first computational results; (ii) then, in section III, the *Radiver* test case is used to quantitatively assess the numerical results obtained with the two corrections.

## II. PHYSICAL ANALYSIS AND MODELING OF RC EFFECTS IN CENTRIFUGAL IMPELLERS

### A. Theoretical analysis of RC effects in centrifugal compressors

As described by Bradshaw [4], system rotation and streamline curvature have a common physical nature: a parallel flow in a rotating frame becomes a curved flow in the absolute frame of reference. However, if curvature is to be considered as *mainly* caused by the geometry, and if rotation is to be assimilated to *system* rotation, then the analysis should be made in the rotating frame of reference.

The first way by which rotation modifies the turbulent activity is known as the shear/Coriolis instability [3]. The analogy between the plane-channel flow with spanwise rotation and the outlet of a centrifugal impeller suggests that the pressure side should be destabilized, while the suction side should be stabilized [11]. A second effect of the Coriolis acceleration is the inhibition of the energy cascade to small scales [12]. In a radial impeller, this would simply lead to a slower decay of turbulence, but this effect is most probably negligible compared to the shear-Coriolis instability.

The effects of streamline curvature on turbulence are well known (see the review of Bradshaw [4]). In the meridional plane of an impeller, the analysis of these effects is rather straightforward: concave hub curvature will increase turbulence intensity, and convex shroud curvature will decrease it. In the blade-to-blade plane, curvature may change along the

chord, preventing a general analysis. However, for the specific case of a backswept impeller, curvature will counteract the effect of rotation in the aft part of the blades.

The outcome of this competition can be estimated by a modified Rossby number, defined as

$$R_{o-\mathrm{m}} = \left| \frac{W \sin \sigma \cos \beta}{\Omega R_c} \right| \equiv \frac{\mathsf{Curvature}}{\mathsf{Rotation}},$$

where $W$ is the magnitude of the relative velocity, $\sigma$ the inclination of the flow paths to the radial direction, $\beta$ the inclination to the tangential direction and $R_c$ the radius of curvature. For the *Radiver* compressor, the following estimates can be made close to the trailing edge: $W \simeq 170$ m.s$^{-1}$, $\sigma \simeq 85°$, $\beta_2^b \simeq -38°$ and $|R_c| \simeq 0.07$ m, leading to a value $R_{o-\mathrm{m}} \simeq 0.6$. Therefore, close to the trailing-edge in the blade-to-blade plane, rotation should theoretically slightly dominate.

## B.  First-order corrections for RC effects

The two recent model corrections selected for the present study are sensitized to rotation through an objective Bradshaw-Richardson number, which is a measure of RC effects valid up to strong RC regimes (as demonstrated in reference 9). So far, the assessment of these two corrections for complex turbomachinery flows remains to be done.

### 1.  Equations of the SARC and YSRC corrections

When applied to the SA model, the Spalart & Shur correction consists in multiplying the production term $\mathcal{P}_{SA} = c_{b1}\tilde{S}\tilde{\nu}$ of the baseline model by the rotation function $f_{r1}$:

$$f_{r1}(r^*, \tilde{r}) = (1 + c_{r1})\frac{2r^*}{1 + r^*}\left[1 - c_{r3}\tan^{-1}(c_{r2}\tilde{r})\right] - c_{r1}.$$

The non-dimensional terms $r^*$ and $\tilde{r}$ are defined as

$$r^* = \frac{\tilde{S}}{\tilde{W}},$$

$$\tilde{r} = \frac{2}{D^4}\mathcal{W}_{ik}S_{jk}\left[\frac{dS_{ij}}{dt} + (\varepsilon_{imn}S_{jn} + \varepsilon_{jmn}S_{in})\Omega_m\right], \tag{1}$$

where $S_{ij}$ and $\mathcal{W}_{ij}$ are the strain-rate and absolute-rotation tensors, respectively:

$$S_{ij} = 0.5\ \left(\frac{\partial U_i}{\partial x_j} + \frac{\partial U_j}{\partial x_i}\right) \quad \text{and} \quad \mathcal{W}_{ij} = 0.5\left[\left(\frac{\partial U_i}{\partial x_j} - \frac{\partial U_j}{\partial x_i}\right) + 2\varepsilon_{mji}\Omega_m\right].$$

4

Objective measures of strain and rotation are then obtained as

$$\tilde{S} = (2S_{ij}S_{ij})^{1/2}, \quad \tilde{\mathcal{W}} = (2\mathcal{W}_{ij}\mathcal{W}_{ij})^{1/2}, \text{ and } D^2 = 0.5(\tilde{S}^2 + \tilde{\mathcal{W}}^2)$$

Finally, the model coefficients are $c_{r1} = 1.0$, $c_{r2} = 12.0$ and $c_{r3} = 1.0$.

The correction of Cazalbou *et al.* consists in sensitizing the model coefficient $C_{\epsilon 2}$ to rotation and curvature through the relation:

$$C_{\epsilon 2} = C_{\epsilon 2}^0 + \frac{C_{\epsilon 2}^0 - 1}{1 + a\widetilde{\mathrm{Ro}}^{3/2}} + C_{\epsilon 2}^0 C_{\mathrm{sc}} \frac{\tilde{S}k}{\epsilon} \left[ \tanh\left(b\widetilde{B_{\mathrm{R}}} + c\right) - d \right], \tag{2}$$

where $\widetilde{Ro}$ is an objective Rossby number defined as

$$\widetilde{Ro} = \frac{\epsilon}{\tilde{\Omega}k}, \quad \text{with} \quad \tilde{\Omega} = (\mathcal{W}_{ij}\mathcal{W}_{ij}/2)^{1/2},$$

and $\widetilde{B_{\mathrm{R}}}$ is the objective Bradshaw-Richardson adapted from the proposition of Spalart and Shur:

$$\widetilde{B_{\mathrm{R}}} = -\frac{2k}{\tilde{S}^3\epsilon} \mathcal{W}_{ik}S_{jk} \left[ \frac{dS_{ij}}{dt} + \Omega_m(\varepsilon_{imn}S_{jn} + \varepsilon_{jmn}S_{in}) \right]. \tag{3}$$

Finally, the constants of the correction are:
$C_{\epsilon 2}^0 = 1.83$, $C_{\mathrm{sc}} = 0.119$, $a = 4.3$, $b = 5.13$, $c = 0.453$ and $d = 0.682$.

## 2. *Implementation issues*

The two RC corrections have been implemented in the Euranus solver of the FINE/Turbo package of Numeca. This multiblock solver is thoroughly presented by Hirsch *et al.* [13]. The Reynolds-Averaged Navier-Stokes equations in the rotating frame are solved with a time-marching method. Time integration is ensured by a 4-stage Runge-Kutta scheme. Local-time stepping and a 3- or 2-level multigrid technique are used to accelerate convergence to the steady state. The discretization in space is based on a cell-centered control-volume approach. Convective fluxes are determined by a second-order centered scheme with added artificial dissipation of the Jameson type. Viscous fluxes are centered. Total quantities and the direction of velocity are imposed at the inlet. At the outlet, the massflow is imposed through a velocity scaling procedure.

Implementing the corrections is rather straightforward since only source terms are involved. First and second derivatives of the velocity field are obtained by successive applications of a finite-volume estimation of the gradients.

To verify the implementation, a specific postprocessing was used, independent of the modifications made to the solver. The calculated values are verified against analytical expressions for three basic flow configurations: (i) initially-isotropic homogeneous rotating turbulence; (ii) homogeneously-sheared rotating turbulence; and (iii) an hypothetical case of increasingly-sheared turbulence with rotation (defined as $W_1 = Kxy$, $W_2 = W_3 = 0$, and $\mathbf{\Omega} = \Omega_0 \mathbf{z}$, where $K$ and $\Omega_0$ are positive constants). The latter case was needed to verify the implementation of second-order derivatives in (1) and (3).

As the YSRC model is concerned, it must be mentioned that equation (2) can return excessively high or low values for the $C_{\epsilon 2}$ coefficient when practical 3D calculations are performed. This is due to the presence of the ratio of the turbulent to mean-flow time scales ($\tilde{S}k/\epsilon$) at the right-hand side of equation (2), that can take unrealistically high values when a $(k, \epsilon)$ model is used. A standard fix (see for instance Menter [14]) is to limit the possible range of variation of this ratio (or equivalently, of the production-to-dissipation ratio). Here we choose to limit directly the variation of $C_{\epsilon 2}$. A selection of upper and lower bounds consistent with the design method of the corrected model gives, at least, $C_{\epsilon 2}^{\max} = 3.17$ and $C_{\epsilon 2}^{\min} = 1.16$ (see appendix A). On the other hand, Menter [14] suggests to limit the ratio of production to dissipation to 10, which can be shown to limit the value of $C_{\epsilon 2}$ to 3.4 on the basis of equation (2). With some margin with respect to these values, the lower and upper bounds retained in the final implementation of the model are $C_{\epsilon 2}^{\min} = 1.1$ and $C_{\epsilon 2}^{\max} = 5$.

### C.   Qualitative analysis for the *Radiver* compressor

#### 1.   Comparison with theoretical considerations

To assess the capability of the corrections to reproduce the expected effects of rotation and curvature on the turbulent field, preliminary computations for the design point of the *Radiver* test case are scrutinized. Since the purpose of this part is not the validation of the computations against experimental data, the presentation of the test case and of the numerical setup is left for the next section. The geometry and the computational grid are represented in figure 1.

We shall first consider the comparison of the turbulent-viscosity fields obtained with the baseline and corrected models. We begin with the meridional mass-averaged fields of

6

normalized turbulent viscosity ($\mu_t/\mu$, the turbulent Reynolds number) presented in figure 2. For both baseline models [figures (a) and (c)], a highly-turbulent region starts just after the leading edge of the blade, in the shear layer at the shroud endwall. Turbulence then extends to form a pocket which occupies almost the whole of the meridional section as it enters the vaneless diffuser. There, the maximum turbulence activity occurs at about mid span for both models. It can be noted here that the absolute level of $\mu_t/\mu$ reaches a higher value with the SA model.

For the SARC model, the impact of curvature can be observed by comparing figures (a) and (b): (i) at the top of the meridional section, the turbulent-viscosity level is significantly reduced due to the convex shroud curvature; (ii) at the bottom of the meridional section, the concave hub surface induces an important turbulence level at about mid-passage, which moves the maximum of turbulent activity closer to the hub. Altogether, these two effects move the maximum turbulence level further into the diffuser.

For the YSRC model, the same impact of convex shroud curvature is observed when comparing figures (c) and (d). However, there is no additional increase due to hub curvature. As a result, the maximum of turbulent viscosity is confined in the immediate vicinity of the shroud surface. This skewness of the turbulent-viscosity field persists in the vaneless diffuser.

Figure 3 illustrates the behavior of the models with a mid-span blade-to-blade view of the turbulent Reynolds number field. For both baseline models, the observed turbulent field results from the production in the shroud area mentioned earlier, with no specific contribution of the blade-to-blade flow. For the SARC model, the main impact of the
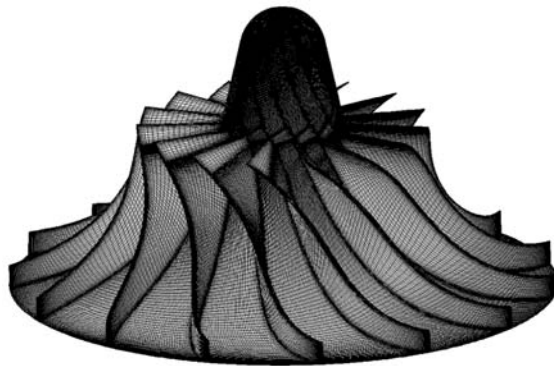


FIG. 1: Three-dimensional view of the *Radiver* impeller with the computational grid.

correction can be seen close to the trailing edge, where the intensity of the normal-to-the-blade component of the Coriolis force is maximum. There, the rotation effect triggers an increase of the turbulent activity at the pressure side of the blade [in the area marked D in figure 3 (b)], in agreement with the expected effects of rotation. The stabilizing effect at the suction side is not so obvious. Thus, the computation results indicate that the SARC model fosters the effect of rotation over the effect of curvature for this case, as was predicted from the Rossby number analysis made earlier.

On the other hand, the effect of rotation is not observable for the YSRC correction in
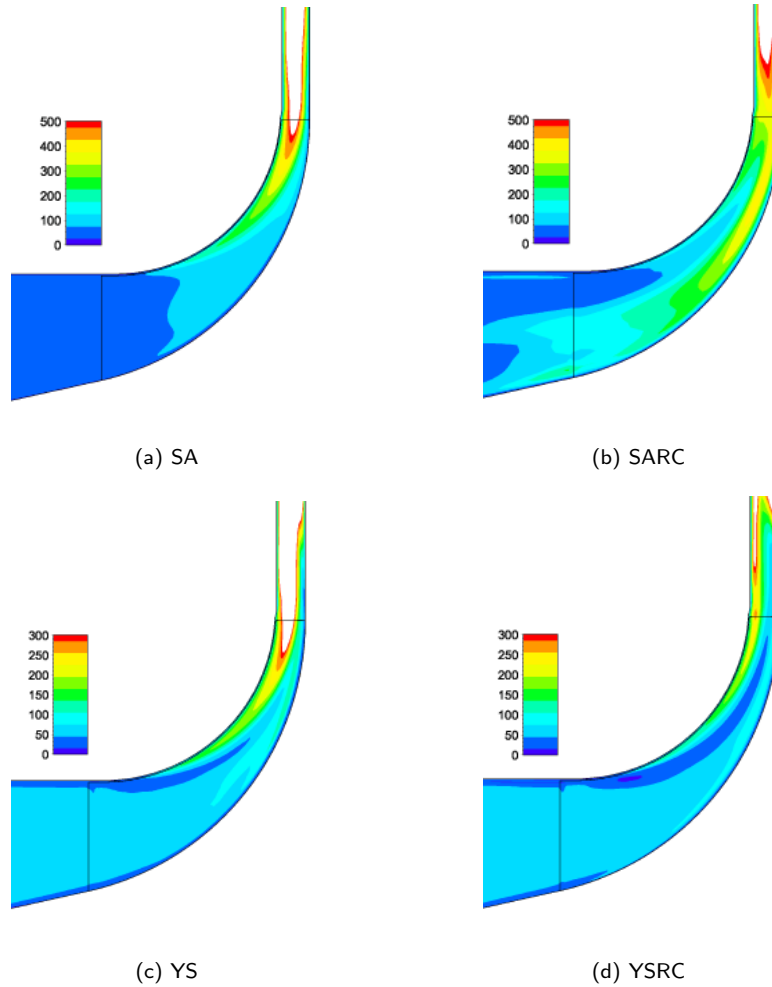


(a) SA

(b) SARC

(c) YS

(d) YSRC

FIG. 2: Meridional view of the mass-averaged field of turbulent viscosity, normalized by the dynamic viscosity $(\mu_t/\mu)$. The two RC corrections reproduce the effect of curvature: turbulence is increased close to the concave hub surface, and reduced near the convex shroud surface. The computational domain is only partially represented, and the color scale are different for the one- and two-equation models.
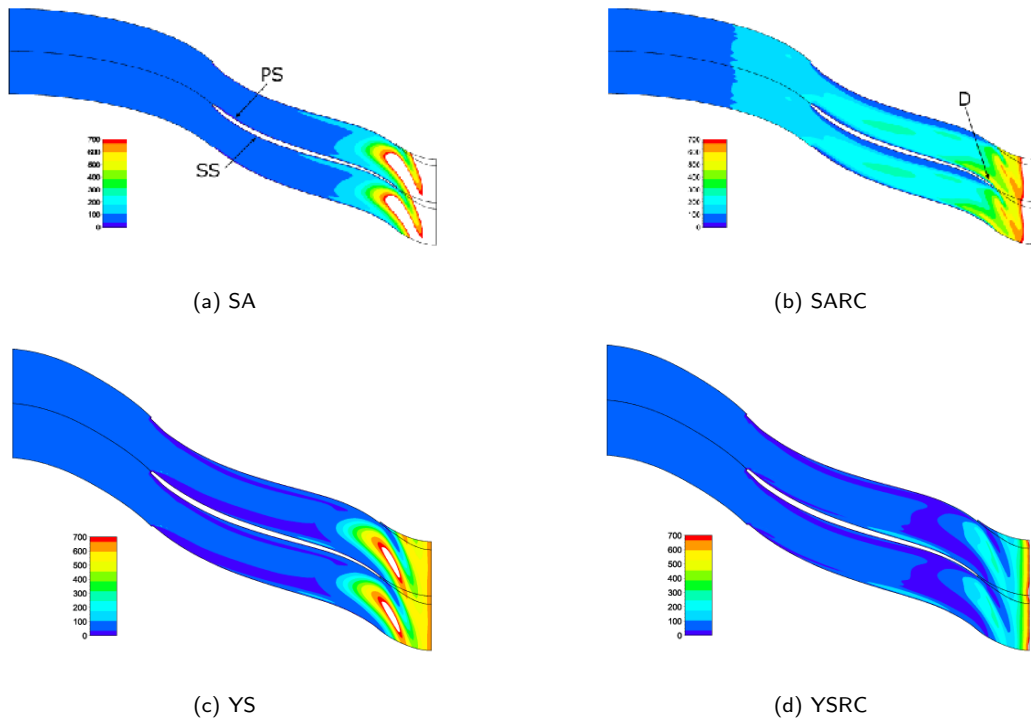
(a) SA

(b) SARC

(c) YS

(d) YSRC

FIG. 3: Mid-span blade-to-blade view of the field of normalized turbulent viscosity $\mu_t/\mu$. The SARC correction reproduces the effect of rotation: turbulence is increased close to pressure-side at the trailing edge (area marked by a D), and reduced near the suction side.
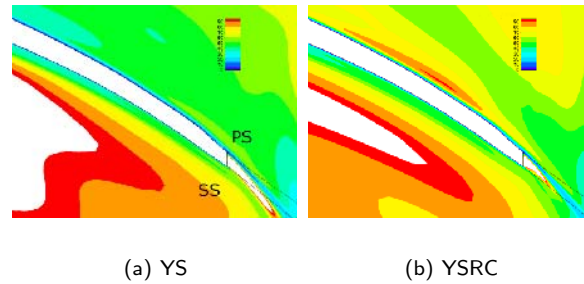


(a) YS

(b) YSRC

FIG. 4: Trailing-edge close up of a 10 % span blade-to-blade view of the field of the normalized turbulent viscosity $\mu_t/\mu$. Contrary to the blade-to-blade midspan of figure 3, here the YSRC correction reproduces the effect of rotation: turbulence is increased close to pressure side at the trailing edge.

figure 3 (d). Figure 4 presents a close-up of the trailing-edge area in a blade-to-blade plane located at 10 % of the span. In this case, the destabilization due to rotation can be observed at the pressure side of the blade, and a slight stabilization is present at the suction side.

Altogether, it can be concluded that there is an excellent agreement between elementary considerations on the effects of rotation and curvature in a centrifugal compressor and the impact of both RC corrections on the prediction of the turbulent field.

## III. VERIFICATION AND VALIDATION FOR THE *RADIVER* TEST CASE

### A. Test case description, computational setup and postprocessing

#### 1. Description of the Radiver test case

The *Radiver* test case is a centrifugal-compressor stage, comprising an unshrouded impeller, a wedge-type diffuser and a downstream collector. The main characteristics of the geometry and the operating point of the compressor are given in table I. An extensive experimental study of this compressor was carried out by Ziegler [15] at the RWTH of Aachen, and is available as an open test case presented in references 16 and 17. The primary goal of this test case is the study of rotor/stator interactions, but a vaneless configuration was also tested. In the present study, we shall only consider the vaneless diffuser cases.

To the authors' knowledge, only two published numerical studies have considered the

TABLE I: *Radiver* test case: geometry and operating point of the compressor.

| Impeller characteristics | | | |
|---|---|---|---|
| Number of blades | $Z_b$ | = | 15 |
| Outlet radius | $R_2$ | = | 135 mm |
| Outlet backsweep angle | $\beta_2^b$ | = | $-38°$ |
| Outlet blade height | $b_2$ | = | 11.1 mm |
| Operating point characteristics | | | |
| Nominal rotation speed | $N_0$ | = | 35200 rpm |
| Maximum corrected massflow | $\dot{m}_{cor}^{max}$ | = | 2.5 kg/s |
| Nominal specific speed | $n_s$ | = | 0.69 |
| Maximum stage pressure ratio | $\pi_{tt}^{max}$ | = | 4.1 |
| Maximum stage isentropic efficiency | $\eta_{is-tt}^{max}$ | = | 0.834 |

*Radiver* test case: Weiß *et al.* [18] computed the vaneless configuration; and Boncinelli *et al.* [19] analyzed the impeller–diffuser interaction.

According to the information given by Ziegler [15], the following experimental uncertainties must be considered: (i) pressure measurements are accurate to 0.2 %; (ii) temperature measurements are accurate to 0.3 %, combining this with the accuracy of pressure measurement, uncertainty analysis yields an accuracy of 0.8 efficiency points for the isentropic efficiency; (iii) L2F measurements are accurate to about 2 % for velocities and 3° for flow angles.

For the geometry modeling, the bulb upstream of the rotor was partially included: Weiß *et al.* [18] report a negligible influence of the inlet duct, and available experimental results suggest that the corresponding pressure loss is less than measurement accuracy. Although results are only extracted just aft of the rotor, the vaneless diffuser was modeled up to a radius about $R = 1.5 \times R_2$. The hot-running conditions are solely accounted for by their impact on the clearance height, as described in references 15 and 18: the gap size was set to 0.684 mm at the leading edge and 0.358 mm at the trailing edge. The blunt trailing edge is fully accounted for.

### 2. *Computational setup*

All computations were run with the numerical setup detailed in section II B 2. Standard iterative-convergence criteria were selected: (i) a reduction of at least 3 orders of magnitude of the rms-residuals; (ii) stabilization of the massflow, with less than 0.1 % difference between inlet and outlet; and (iii) stabilization of the global quantities of interest (pressure ratio and efficiency). The uncertainty associated to iterative convergence was graphically estimated [20], and found to be negligible.

### 3. *Postprocessing of the numerical results*

Particular care was devoted to ensure to match the numerical postprocessing with the experimental procedure. The total–total pressure ratio of the rotor was postprocessed using discrete values of total pressure extracted on a constant-radius surface in the channel ($R$=138.1 mm) after a mass-weighted azimuthal averaging, combined with average static-

pressure values extracted at specific locations for the hub and shroud ($R$=137.5 mm and $R$=138.8 mm respectively). The L2F measurement plane was reproduced according to the definition given in reference 16. However, the "Hi-3" experimental procedure for the extraction of total temperature, designed to account for heat fluxes through the shroud endwall, is replaced by a standard mass-averaged extraction in the adiabatic simulations.

## B.   Verification of the solutions

### 1.   Mesh parameters

Before conducting the grid-convergence study, the selection of mesh parameters was made according to Dufour *et al.* [21]. Based on the fact that different flow characteristics converge at different rates, the study of reference 21 uses the design of experiment technique to quantify the influence of different mesh parameters on selected flow quantities. A specific outcome of this study was the demonstration of the determining influence of the tip-gap discretization on the shroud friction coefficient, further quantified in reference 22: for a centrifugal compressor similar to the *Radiver*, convergence of the shroud friction coefficient within a 5 % numerical-error band requires at least 37 grid points between the blade tip and the shroud in the spanwise direction.

Based on these preliminary studies, a reference mesh of 3 million cells was generated. To perform grid-convergence tests, the number of grid points in each direction was halved. However, this is too high a coarsening to ensure an accurate grid-convergence study (a factor $r_h = 1.3$ in each direction is advised by Celik [23]). Therefore, a 1.5 million-cells grids was generated, to which a coarsening of $r_h = 2$ was again applied. All grids use an HI 4-block topology, which consists of one block in the blade passage, two blocks for the butterfly mesh in the tip gap, and one block downstream the blunt trailing edge. Table II summarizes all the grids used.

By construction, grid coarsening is uniform between grids A and C on one hand, and grids B and D on the other. However, there is some degree of non-uniformity between grids A and B (and consequently between C and D). This issue, mentioned in reference 20 is not investigated in the present study.

12

TABLE II: *Radiver* test case: characteristics of the grids used for mesh-convergence studies. The numbers of points for each block are given in the following form: azimuthal×spanwise×streamwise.

| Grid nomenclature | Number of points | | | | |
| --- | --- | --- | --- | --- | --- |
| | Total | Blade passage | Tip gap (H) | Tip gap(C) | Downstream blunt |
| Grid A | 2 992 036 | $81 \times 97 \times 313$ | $25 \times 42 \times 273$ | $17 \times 41 \times 129$ | $41 \times 97 \times 41$ |
| Grid B | 1 555 620 | $65 \times 77 \times 249$ | $17 \times 33 \times 273$ | $17 \times 33 \times 129$ | $33 \times 73 \times 33$ |
| Grid C | 386 708 | $41 \times 49 \times 157$ | $13 \times 21 \times 137$ | $9 \times 21 \times 65$ | $21 \times 49 \times 21$ |
| Grid D | 203 052 | $33 \times 39 \times 125$ | $9 \times 17 \times 137$ | $9 \times 17 \times 65$ | $17 \times 39 \times 17$ |

### 2.  Numerical error estimation

The four models were run on the grids A to D, for 5 operating points (P1, P2, M, S2 and S1 from the lowest to the highest massflow on the $N = 0.8 \times N_0$ speed line, see figure 6). However, iterative convergence problems appeared with the $(k, \epsilon)$ models on grid A, for which large oscillations of global quantities (higher than 2 %) were observed. The corresponding results are therefore not shown here. This problem may be due to the fact that a very fine grid fosters the appearance of small flow structures, thus questioning the existence of a steady solution.

Figure 5 synthesizes the grid-convergence results for all the models, for three operating points (P1, M and S1). The results obtained with the three finest grids available for each model are used to apply the extrapolation of Richardson and compute the "estimated (relative) error" ($\delta_{RE}$), as well as the "observed order of accuracy" ($p_{obs}$), according to the procedures described in reference 23 for instance. The results are displayed in log–log scale, with $h$ an average cell size, defined as $h = $ (Total number of points)$^{-1/3}$. $h_{max}$ corresponds to grid D.

It must first be mentioned that the resolution of the key physics on each grid level was checked. We examined three important features: the three-dimensional meridional separation leading to the formation of the wake, the presence of a tip-leakage vortex and the development of strong secondary flows. Theses phenomenon were qualitatively observed for all the grids.

For the baseline models, the coarsest grid (200 000 points) yields errors of about 2 % for the pressure ratio and 3 points for the efficiency. Beyond 1.5 million points, the pressure

(a) Operating point P1      (b) Operating point M      (c) Operating point S1

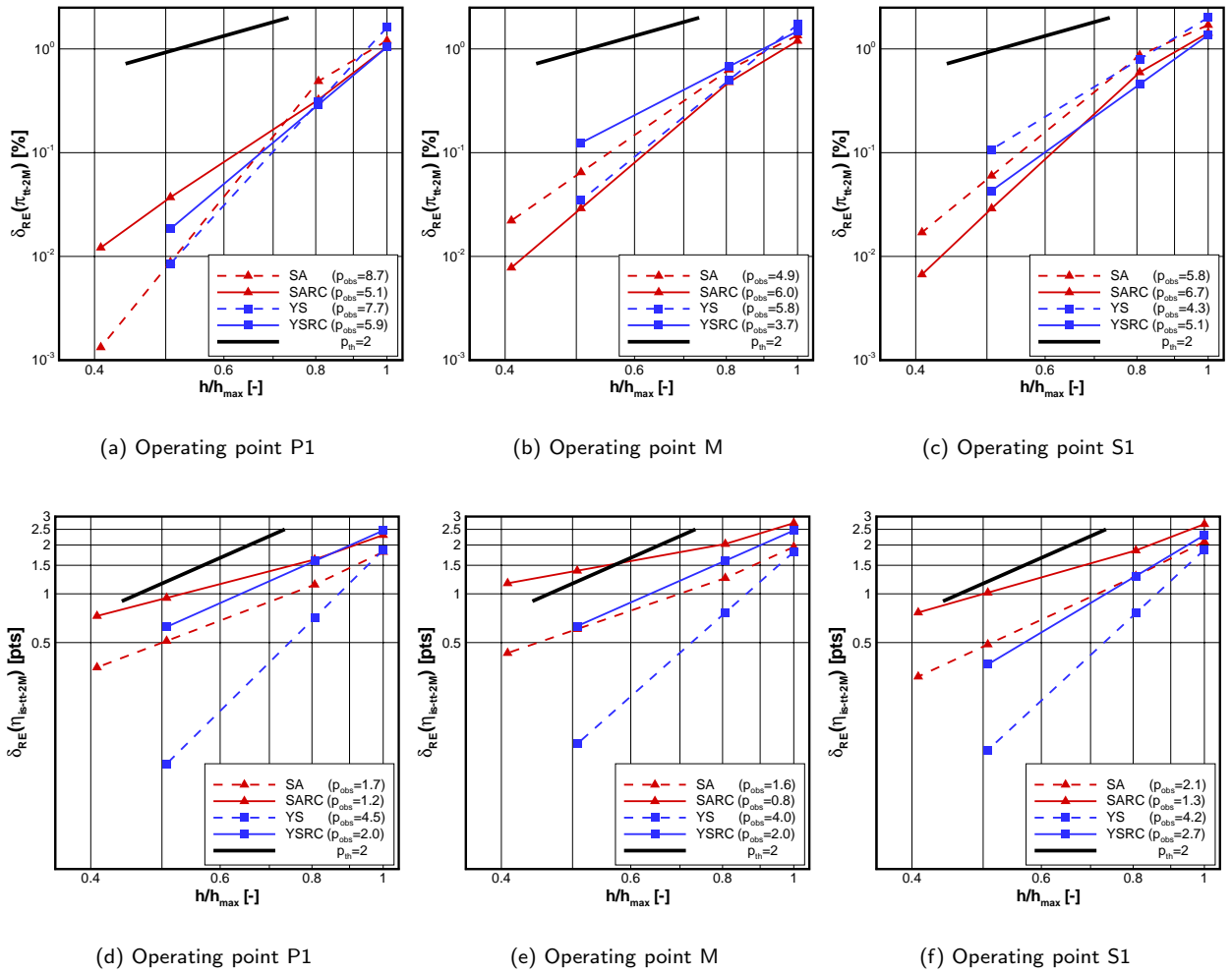(d) Operating point P1      (e) Operating point M      (f) Operating point S1

FIG. 5: Numerical errors for the total–total pressure ratio and isentropic efficiency, estimated by the Richardson extrapolation. Estimated errors are expressed in percentage of the extrapolated values for the pressure ratio, and in efficiency-points decrements with respect to the extrapolated value for the efficiency. The values of the observed order of accuracy are given in the legends.

ratio reaches grid convergence (at least within 0.1 % relative error), while there is still about a one-point error for the efficiency. The errors appear as higher for the one-equation models, which contrasts with results reported elsewhere in other flow configurations [24].

The influence of the RC corrections on the numerical error does not exceed 0.5 % for the prediction of the pressure ratio. For the efficiency, the two corrections increase the numerical error of about 0.5 points for all the operating points considered. It can also be noted that the corrections slightly modify the grid-convergence rate: the observed order of accuracy is lower for many of the predictions with the corrected models (see the legends in figure 5).

14

Interestingly, it seems that there is a very weak influence of the operating point on the numerical errors: in other words, it appears that for this specific test case, the classical statement that "tendencies" can be well predicted with relatively coarse grids is substantiated.

## C. Validation

The results obtained with grid B are now presented to allow consistent comparisons of the four models on the same mesh. Experimental uncertainties are figured with two-sided error bars.

### 1. Global performances

Figure 6 compares numerical and experimental results for the global performances. For all models, the pressure ratio is overestimated by 0.7 to 2 %, but with a very good prediction of the trend. Efficiency is underestimated by 0.5 to 1 point, with a noticeable difference in the trend.

To quantify the impact of the corrections with a minimum bias, we shall use the notion of



(a) Total–total pressure ratio at plane 2M

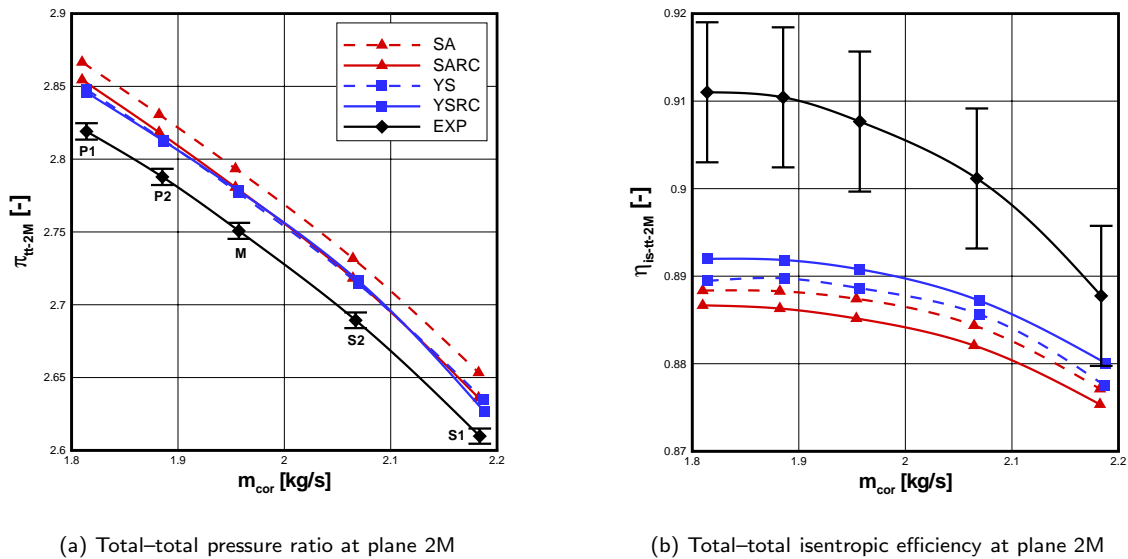(b) Total–total isentropic efficiency at plane 2M

FIG. 6: Comparison of the global performances obtained with the baseline and RC-corrected models against experimental values for the *Radiver* test case. Numerical results obtained on Grid B.

15

the "validation uncertainty", proposed by Coleman and Stern [25]. Since then, this notion has been used to form "validation metrics", and has been extended in many publications (see for instance reference 26). The validation uncertainty, denoted $U_{\mathrm{VAL}}$, is defined as the root-mean-square of all the uncertainties that can be estimated. As put by Coleman [27], we shall consider that $U_{\mathrm{VAL}}$ sets the best "level of validation" possible: any comparison below $U_{\mathrm{VAL}}$ is not significant from an uncertainty point of view. If the comparison $E$ is defined as the difference between the experimental and numerical values, the level of validation $L_{\mathrm{VAL}}$ is finally defined as $L_{\mathrm{VAL}} = \max(|E|, U_{\mathrm{VAL}})$.

In our case, $U_{\mathrm{VAL}}$ involves the numerical ($U_{\mathrm{NUM}}$) and experimental ($U_{\mathrm{EXP}}$) uncertainties, according to: $U_{\mathrm{VAL}} = \sqrt{U_{\mathrm{EXP}}^2 + U_{\mathrm{NUM}}^2}$. Assuming that numerical errors and uncertainties are equivalent, validation results are synthesized in table III. The uncertainty evaluation is presented only for the nominal operating point (M), but similar results were obtained for the other points of operation.

Regarding the uncertainty analysis in the V&V framework, the significance of the impact of the corrections must be assessed by comparing $\Delta$RC (the variation of a global quantity between the baseline and the corrected models) and $U_{\mathrm{VAL}}$ (the best level of validation possible). According to the results given in table III, it appears that only the variation of the predicted pressure ratio for the SARC model is above $U_{\mathrm{VAL}}$. In this case, a very slight

TABLE III: *Radiver* test case: validation results for the nominal operating point (M). All the differences and uncertainties are expressed as a percentage of the experimental value for the pressure ratio, and as efficiency-point decrements for the isentropic efficiency. Comparing $U_{\mathrm{VAL}}$ and $\Delta$RC gives the significance of the impact of the RC corrections.

|  |  | SA | SARC | YS | YSRC |
|---|---|---|---|---|---|
| $\pi_{tt-2M}$ | $E$ | 1.55 | 1.09 | 0.95 | 1.00 |
|  | $U_{\mathrm{VAL}}$ | 0.21 | **0.20** | 0.20 | **0.24** |
|  | $\Delta$RC | – | **0.46** | – | **-0.05** |
|  | $L_{\mathrm{VAL}}$ | 1.55 | 1.09 | 0.95 | 1.00 |
| $\eta_{is-tt-2M}$ | $E$ | 2.02 | 2.25 | 1.90 | 1.69 |
|  | $U_{\mathrm{VAL}}$ | 1.00 | **1.60** | 0.81 | **1.02** |
|  | $\Delta$RC | – | **-0.22** | – | **0.21** |
|  | $L_{\mathrm{VAL}}$ | 2.02 | 2.25 | 1.90 | 1.69 |

improvement of about 0.5 % is observed, which is about one third the difference between the SA model predictions and the experimental data. For all the other cases, the impact of the corrections is negligible, since it is lower than the sum of the experimental and numerical uncertainties.

Therefore, it must be concluded that the RC corrections evaluated here do not have a significant impact on the prediction of global quantities for the *Radiver* test case. Nevertheless, for all the models tested the validation level achieved is at best 0.95 % for the pressure ratio and 1.69 points for the efficiency.

### 2. *Azimuthally-averaged profiles*

A comparison of experimental and numerical results for the azimuthally-averaged profiles of total pressure at rotor outlet is presented in figure 7. All the models yield a rather good prediction for all the operating points. The main discrepancies appear at the frontier between the jet and wake structures (roughly at $Z/B = 0.5$), where there seems to be too strong a mixing to capture the steep gradients.

Again, the notion of validation uncertainty is used to assess the impact of the RC corrections. In this case, both the numerical and the experimental uncertainties are low (as previously mentioned, $U_{\mathrm{EXP}} \simeq 0.2$ %; and the numerical uncertainty assessed does not ex-



(a) Operating point P1          (b) Operating point M          (c) Operating point S1
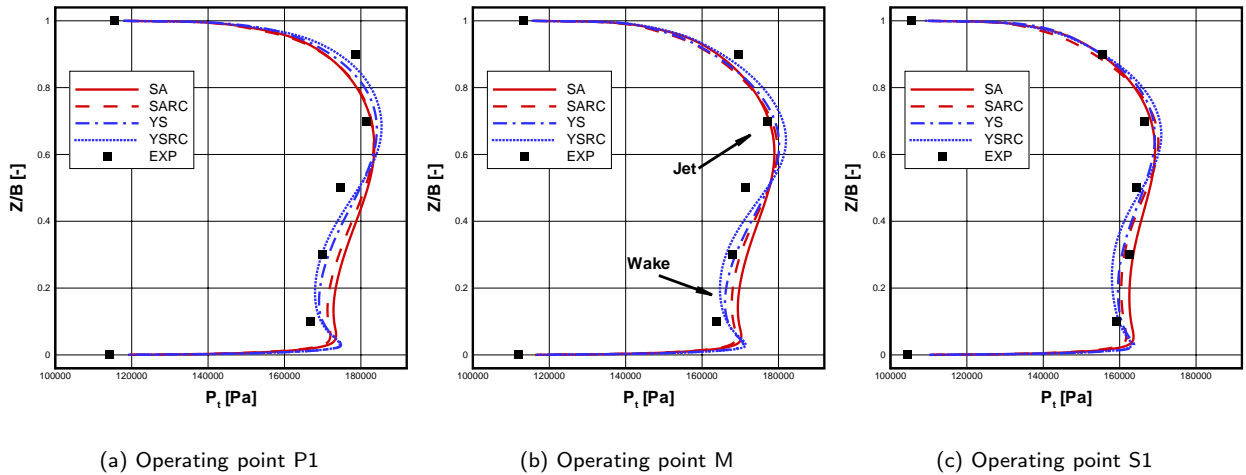
FIG. 7: Comparison of experimental and numerical azimuthally-averaged profiles of total pressure. Computational results obtained on Grid B. Experimental- and numerical-uncertainty error bars are smaller than the symbols at the scale of the figure.

17

ceed 0.12 %). Therefore, the level of validation achieved for the total-pressure profiles is about 0.25 % at maximum. Qualitatively, this amounts to an uncertainty band whose size is smaller than that of the symbols in figure 7. A mean impact of the corrections can be obtained with the root-mean-square of the changes between the SA and SARC profiles (defined as $\Delta_{\mathrm{RMS}} = \sqrt{1/n \sum_{k=1}^{n} (\phi_k^{SARC} - \phi_k^{SA})^2}$, where $\phi_k$ is the considered quantity at the $k^{\mathrm{th}}$ spanwise location), which is about 1 % (note that there is some compensation between the opposite variations at the hub and shroud). It can thus be concluded here that the impact of the correction is significant for the predictions of the total-pressure profiles. More specifically, the correction gives a better prediction of the *extrema* close to the hub and shroud. The L2 norm of the changes between the YS and YSRC profiles is about 0.9 %, still higher than the level of validation. Again, the correction yields an improved prediction of the *extrema*, in better agreement with the experimental results.

Altogether, uncertainty analysis shows that the corrected models improve the comparison with the experimental results, most probably due to a better prediction of the jet/wake composite profiles. This tends to confirm the contribution of turbulence RC effects to the formation of the jet/wake structure as conjectured by Baljé.

Figure 8 compares numerical results with L2F measurements in the form of azimuthally-averaged profiles. Only the operating point P1 is considered as it is the only one for which L2F data are available. For all the flow quantities considered, it can first be directly observed



(a) Absolute tangential velocity     (b) Relative flow angle     (c) Relative velocity magnitude
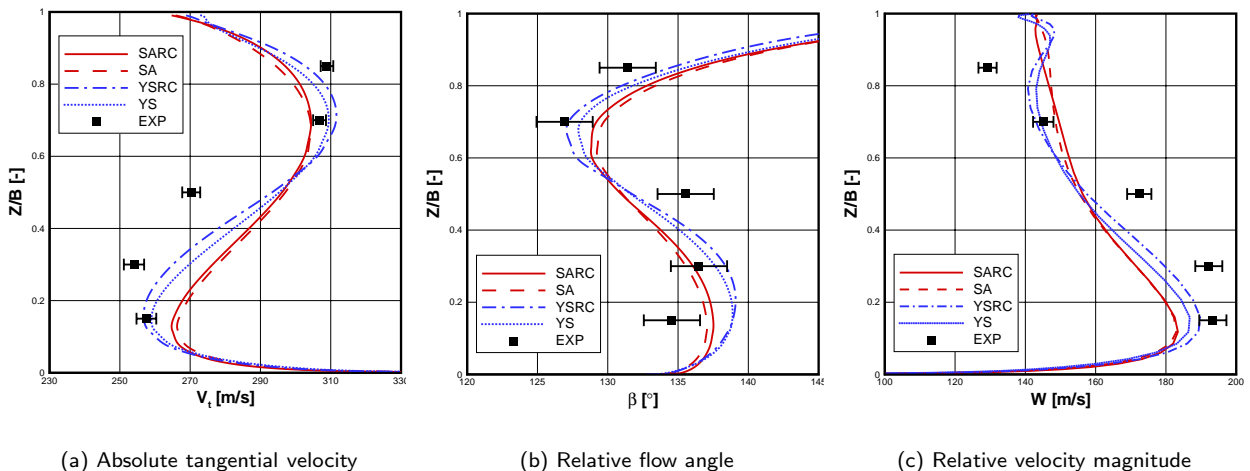
FIG. 8: Comparison of L2F-experimental and numerical azimuthally-averaged profiles for the operating point P1. Computational results obtained on Grid B.

that the experimental uncertainty alone exceeds the impact of the corrections. Therefore, a first conclusion is that, from an uncertainty point of view, the impact of the corrections is not significant for azimuthally-averaged profiles of kinematic quantities.

For the absolute tangential velocity (a), significant discrepancies are observed between predictions and experiments, with fair agreement only close to the hub and the shroud. At midspan, the differences are consistent with the underestimation of the pressure ratio and efficiency, as it indicates a deficit of work exchange. The prediction of the relative flow angle is only slightly better (b), indicating a rather different flow structure in the predictions. Finally, the comparison of the relative-velocity profiles (c) globally connects these discrepancies with the prediction of the jet/wake structure, which appears to undergo too much mixing.

### 3. 2D Fields

Figure 9 presents color contours of relative velocity magnitude at the rotor outlet , for the operating point P1. The comparison confirms that the slight improvements associated to the RC corrections for the total-pressure profiles are indeed connected to a qualitatively better prediction of the jet/wake structure. It appears that the RC-corrected models predict a larger extension of the wake pocket close to the shroud, together with a more pronounced jet close to the pressure side at the hub. The $(k, \epsilon)$ models yield slightly better pressure profiles thanks to a lower mixing, which appears here in the form of a larger difference between maximum and minimum velocity levels. This is even more pronounced for the YSRC model, with a significantly larger extension of the wake pocket close to the suction side.

Altogether, these flowfields clearly show that much of the impact of the correction manifests with opposite effects on the pressure and suction sides, which cancels when azimuthally averaged.

## IV. SYNTHESIS AND CONCLUSIONS

The present study has examined the physics and the modeling of rotation and curvature effects on turbulence, and their impact on the flow in a centrifugal compressor. The litera-
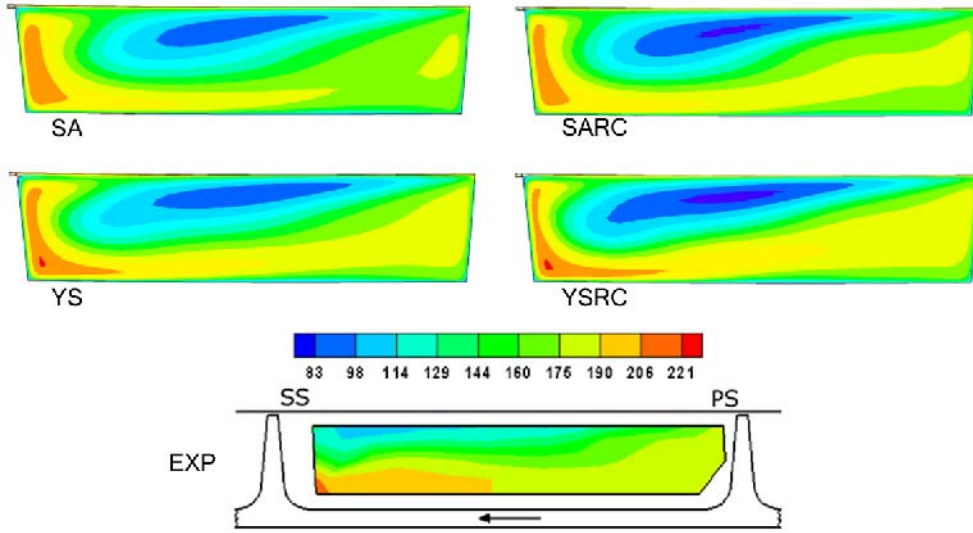
FIG. 9: Comparison of predictions and L2F measurements for the relative velocity at rotor outlet (operating point P1). Computational results obtained on Grid B. Color scale given in m/s.

ture shows that known RC effects in basic configurations motivate a detailed analysis in radial turbomachinery configurations. Given the defects of many existing RC corrections for classical turbulence models, we have implemented two recent corrected models that are sound from both a mathematical and physical point of view. The assessment of the impact of these two corrections for the prediction of the *Radiver* test case has been carried out within the verification and validation framework.

The consistency of the two corrections is demonstrated: the numerical predictions are in perfect agreement with the targeted physics. The stabilization and destabilization areas induced by rotation and curvature are reproduced by the corrections, through a significant modification of the turbulent-viscosity field. However, uncertainty analysis shows that the impact of the corrections on global performances is negligible. Locally, slight improvements (about 1 %) are observed for azimuthally-averaged profiles of total pressure, but flow angles and velocity components are not significantly impacted. Analysis of a 2D field of the relative velocity shows a noticeable impact, and confirms the previously hypothesized impact of turbulence RC effects on the formation of the jet/wake structure at rotor outlet. Taking into account global and local predictions, it appears that all the models studied here yield a fairly good agreement with experiments, although it can be argued that a slightly better prediction of local properties is obtained with the YSRC model.

Our analysis of the rather limited impact of the corrections for this particular test case is the following:

- The dissymetry (between pressure and suction side on one hand, and hub and shroud on the other) of this impact suggests that averaging may hide some of the effect of the corrections. This prompts the study of a multistage configuration, where the skewness of the flowfield at the rotor exit would impact downstream stages.

- As opposed to the rotating plane-channel flow, it appears that in this case, the *direct* impact of rotation and curvature on global flow characteristics dominates the *indirect* effect *via* the turbulent field.

Generalization of these conclusions should involve other test cases. The authors have applied the baseline and corrected models to an industrial centrifugal compressor of comparable characteristics, and obtained similar results. We suspect that a more pronounced impact on global predictions could be obtained for impellers with significantly different specific speed and/or flow coefficients, as these two characteristics are closely related to a rotation number. In such cases, the corrections could trigger a change of the flow regime, and thus entail a more sizable global impact.

**APPENDIX A: LIMITING OF $C_{\epsilon 2}$ FOR THE $(k, \epsilon)$ RC CORRECTION**

The limitation of $C_{\epsilon 2}$ is made so that it does not affect the calibration case of homogeneously-sheared rotating turbulence. To this end, we recall here the model problem in that case:

$$\frac{dk}{dt} = C_\mu \frac{k^2}{\epsilon} S^2 - \epsilon \quad ,$$
$$\frac{d\epsilon}{dt} = C_\mu C_{\epsilon 1} k S^2 - C_{\epsilon 2} \frac{\epsilon^2}{k} \quad ,$$

which can be combined as

$$\frac{d\alpha}{dt^*} = C_\mu \left( C_{\epsilon 1} - 1 \right) - \left( C_{\epsilon 2} - 1 \right) \alpha^2 \equiv \Lambda(\alpha) \quad , \tag{A1}$$

where $t^* = St$. With $\alpha(0) = \alpha_0 = \epsilon_0/(Sk_0)$, equation A1 constitutes a fully-defined dynamical system for the state variable $\alpha$. Its fixed points $\alpha_\infty$ are the solutions to the equation

$\Lambda(\alpha) = 0$. Since $C_{\epsilon 2}$ is the only model coefficient made sensitive to rotation, the following relation holds at the fixed point:

$$C_{\epsilon 2} = 1 + C_\mu \frac{C_{\epsilon 1} - 1}{\alpha_\infty^2} \quad . \tag{A2}$$

To preserve the behavior of the model in this situation, the limits of $C_{\epsilon 2}$ must be coherent with the limits of the fixed point. In the fixed-point diagram of the final correction (figure 5 of reference 9), these values are:

- $\alpha_\infty^{min} = \sqrt{3C_\mu/2} = 0.37$, which is the realizability bound of the model;

- $\alpha_\infty^{max} = 0.5$.

Using equation (A2), these values give the following upper and lower limits for the corrected model coefficient: $C_{\epsilon 2}^{max} = 3.17$ and $C_{\epsilon 2}^{min} = 1.16$.

[1] B. Lakshminarayana, Turbulence modeling for complex shear flows, AIAA J. **24**(12), 1900–1917 (1986).

[2] P. Bradshaw, Turbulence modeling with application to turbomachinery, Prog. Aerospace Sci. **32**, 575–624 (1996).

[3] D. J. Tritton, Stabilization and destabilization of turbulent shear flow in a rotating fluid, J. Fluid Mech. **241**, 503–523 (1992).

[4] P. Bradshaw, Effects of streamline curvature on turbulent flows, AGARD (Agardograph 169) (1973).

[5] O. E. Baljé, *Turbomachines, a guide to design, selection and theory*, Wiley, New-York, 1981.

[6] J. Moore and J. G. Moore, Effects of curvature and rotation on turbulence in the NASA low-speed centrifugal compressor impeller, in *Proc. of the 4th Annual Review Meeting of the Center for Turbomachinery and Propulsion Research*, Blacksburg, VA, 1990, Virginia polytechnic institute and state university.

[7] P. R. Spalart and M. L. Shur, On the sensitization of turbulence models to rotation and curvature, Aerospace Science and Technology **1**(5), 297–302 (1997).

[8] P. R. Spalart and S. R. Allmaras, A one-equation turbulence model for aerodynamic flows, La Recherche Aérospatiale **1**, 5–21 (1994).

[9] J.-B. Cazalbou, P. Chassaing, G. Dufour, and X. Carbonneau, Two-equation modeling of turbulent rotating flows, Phys. Fluids **17**(055110) (2005).

[10] Z. Yang and T. H. Shih, A $k,\epsilon$ model for turbulence and transitional boundary layer, in *Near-wall turbulence flows*, edited by C. G. Speziale and B. E. Launder, Elsevier-Science, 1993.

[11] J. P. Johnston, Effects of system rotation on turbulence structure: a review relevant to turbomachinery flows, Int. J. of Rotating Machinery **4**(2), 97–112 (1998).

[12] R. S. Rogallo, Numerical experiment in homogeneous turbulence, Technical Report TM 81315, NASA, 1981.

[13] C. Hirsch, C. Lacor, C. Dener, and D. Vucinic, An integrated CFD system for 3D turbomachinery applications, AGARD-CP-510 (1991).

[14] F. R. Menter, M. Kuntz, and R. Langtry, Ten years of industrial experience with the SST

turbulence model, in *Turbulence, heat and mass transfer 4*, edited by K. Hanjalić, Y. Nagano, and M. Tummers, Begell House, Inc., 2003.

[15] K. U. Ziegler, *Experimentelle untersuchung der Laufrad-Diffusor-Interaktion in einem Radialverdichter variabler Geometrie (In German)*, Shaker Verlag, Ph.D. thesis, RWTH Aachen, 2003.

[16] K. U. Ziegler, H. E. Gallus, and R. Niehuis, A Study on impeller diffuser interaction. Part I: Influence on the performance, ASME Trans. J. Turbomach. **125**, 173 (2003).

[17] K. U. Ziegler, H. E. Gallus, and R. Niehuis, A Study on Impeller Diffuser Interaction. Part II: Detailed flow analysis, ASME Trans. J. Turbomach. **125**, 183 (2003).

[18] C. Weiß, D. R. Grates, H. Thermann, and R. Niehuis, Numerical investigation of the influence of the tip clearance on the wake formation inside a radial impeller, in *Proc. of the ASME Turbo Expo 2003, USA*, number GT2003-38279, 2003.

[19] P. Boncinelli, M. Ermini, S. Bartolacci, and A. Arnone, Impeller–diffuser interaction in centrifugal compressors: Numerical analysis of the "Radiver" test case, in *Proc. of the 25th AIAA Aerodynamic Measurement Technology and Ground Testing Conference, San Francisco, USA*, number AIAA 2006-3453, 2006.

[20] F. Stern, R. Wilson, H. W. Coleman, and E. G. Paterson, Verification and validation of CFD simulations: Part 1- Comprehensive methodology, ASME Trans. J. Fluids Eng. **123**(4) (2001).

[21] G. Dufour, X. Carbonneau, P. Arbez, J.-B. Cazalbou, and P. Chassaing, Mesh-generation parameters influence on centrifugal-compressor simulation for design optimization, in *Proc. of the 2004 ASME Heat Transfer/Fluids Engineering Summer Conference, Charlotte, USA*, number HT-FED2004-56314, 2004.

[22] G. Dufour, X. Carbonneau, P. Arbez, J.-B. Cazalbou, and P. Chassaing, Numerical-error evaluation for tip-clearance-flow calculations in a centrifugal compressor, in *Proc. of the XXI ICTAM Conference, Poland*, number 12510, 2004.

[23] I. B. Celik and J. Li, Assessment of numerical uncertainty for the calculations of turbulent flow over a backward-facing step, Int. J. for Numerical Methods in Fluids **49**, 1015–1031 (2005).

[24] P. J. Huang, Validation of turbulence models – Uncertainties and measures to reduce them, in *Proc. of the ASME Fluids Engineering Division Summer Meeting, Vancouver, Canada*, number FEDSM97-3121, 1997.

[25] H. W. Coleman and F. Stern, Uncertainties in CFD code validation, ASME Trans. J. Fluids Eng. **119**, 795–803 (1997).

[26] W. L. Oberkampf and M. F. Barone, Measures of agreement between computation and experiment: Validation metrics, J. of Computational Physics **217**, 5–36 (2006).

[27] H. W. Coleman, Some observations on uncertainties and the verification and validation of a simulation, ASME Trans. J. Fluids Eng. **125**, 733–735 (2003).